Lux junior 2024

17. Internationales Forum für den lichttechnischen Nachwuchs
Ilmenau, 6. – 8. September 2024
DOI (proceedings): 10.22032/dbt.61636

DOI: 10.22032/dbt.xxxxx

Possibilities of the Finite-Difference Time-Domain Method for Hybrid Optical Simulations

Dominik Metzner[1]

1 L-LAB – Instute for automotive lighting and mechatronics

Abstract

The purpose of this article will be to find a basis for a connection of Ray Tracing simulations and wave propagation methods using Finite-Difference Time-Domain simulations. Since Ray Tracing uses geometric optic only refractive optics is considered. However, in modern lighting systems the optical elements become increasingly smaller resulting in the occurrence of diffractive phenomena. Those phenomena cannot be considered using Ray Tracing simulations. Further possibilities using a Finite-Difference Time-Domain methods to characterize the scattering behavior after the wave passes the optical element and analyse material parameters will be listed.

Index Terms: Ray Tracing, Wave Propagation, Hybrid Optical Simulation

1 Introduction

Light shaping is becoming increasingly important in various fields, including the automotive industry. Using lens projection systems or simple reflector elements light can be modulated to a certain distribution [1]. To simulate those light distriutions resulting from such systems, only refractive optics has to be taken into account. In modern lighting systems for example in headlight systems the same procedure is used. However, as structures designed to shape light become increasingly smaller, it is necessary to consider not only refractive optics but also diffractive effects. Therefore, a hybrid optical simulation (HOS) approach is investigated, where parts of the optics that involve diffraction are not calculated using ray tracing (RT) but rather through an appropriate wave propagation method. Those kind of diffraction phenomena can be observed using a Finite-Difference Time-Domain (FDTD) algorithm [2, 3]. This method visualize not only the behavior of the propagating wave through a micro-sclaed material surface but it gives many more useful applications about the material and the resulting scattering pattern in the corresponding diffraction orders [4-7]. Within this article a combination

© 2024 by the authors. – Licensee Technische Universität Ilmenau, Deutschland.

This is an **Open Access** article distributed under the terms of the Creative Commons Attribution ShareAlike-4.0 International License, (https://creativecommons.org/licenses/by-sa/4.0/).

method of RT and FDTD and a conclusion of useful applications and possibilities of a FDTD simulation is presented to show how powerful this tool actually is.

2 Procedure and Approaches

Starting the general purpose of a HOS approach with the planned procedures of combining RT and wave propagation followed by the introduction in RT. To evaluate different diffraction effects resulting from the nature of the micro structured surfaces of different optical elements, we have to separate areas on the substrate surface into diffraction causing structures and non-causing structures. For those areas where interference effects can be expected, the FDTD method is introduce to observe the scattering on the material surface an the behavior of the propagating wave through the material.

2.1 Hybrid Optical Simulation Approach

The exact procedure of combining of the HOS approach is illustrated in Fig. 1. Here, Leiner et Al. considered three areas of interest separated in [2]. The first area describes the RT simulation, the second area considers the classification of the macro and nano regimes at the hybrid diffraction optical element (HDOE) where diffraction effects occur. The third area describes the far field after the ray tracing and wave propagation simulation. Shown in Fig. 1 two different programming environments create the HOS approach. The RT method using Helios shown in area 1 and 3 uses c++ while the wave propagation method is initially based on MATLAB according to R. Rumpf in [3].

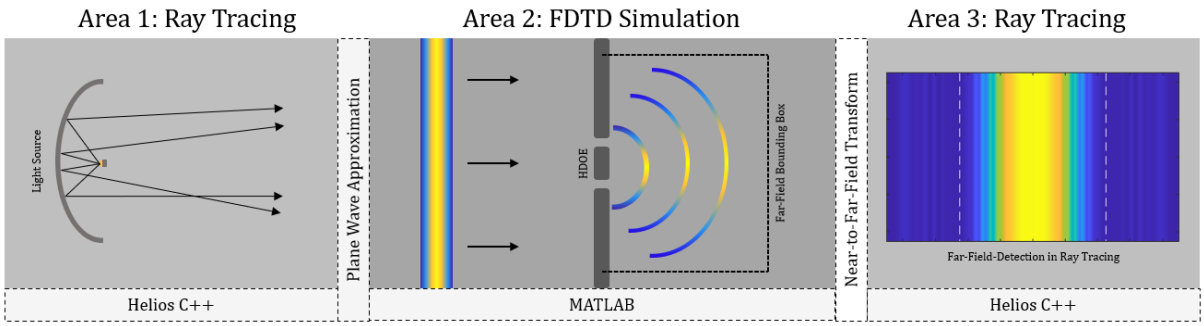

Figure 1: Visualization of the separated simulation areas. Area 1 shows the beginning of the procedure using Ray Tracing simulations with Helios coded in c++. Area 2 describes the wave propagation method (FDTD) using MATLAB. Area 3 shows the re-transform to the detection via Helios in c++. The first interface between area 1 and 2 illustrates the translation of the rays to a plane wave using Plane Wave Approximation. The second interface between area 2 and 3 illustrates a Near-to-Far-Field Transform to translate the FDTD detection into a Ray Tracing result.

To combine those methods to a HOS approach a suitable approximations for the first interface translating a bundle of rays in Helios to a wavefront propagating to the diffractive optical

©2024 by the authors. – Licensee Technische Universität Ilmenau, Deutschland.

element (DOE) has to be defined. To investigate this, a plane wave approximation is performed. For the second interface translating the field from the wave propagation method back to Helios we use a near-to-far-field transform. [8, 9] A combination of both methods results in a highly powerful tool regarding to further possibilities resulting from the FDTD methods shown in Sec. 3.

2.2 Introduction to Ray Tracing

The basis for the following investigations is build by Helios, a 3D ray tracing tool for lighting systems. Within this software, CAD models of an optical element can be inserted and are displayed in a threedimensional simulation space. For the observation of resulting light distruibutions caused by the inserted optical element, different types of light sources, reflector elements and lenses can be added to the simulation. Based on the light source a certain number of rays are traveling parallel or divergent into the simulation space onto the optical element to form the light into a desired distribution. An example of a typical use case of Helios is shown in Fig 2. Here, a divergent LED light source with an reflector element and an aperture to shape the light into the low beam distribution is considered. A lens focusing the light onto the detector surface. Fig. 3 shows the intensitiy of resuting low beam distribution in the far field domain.

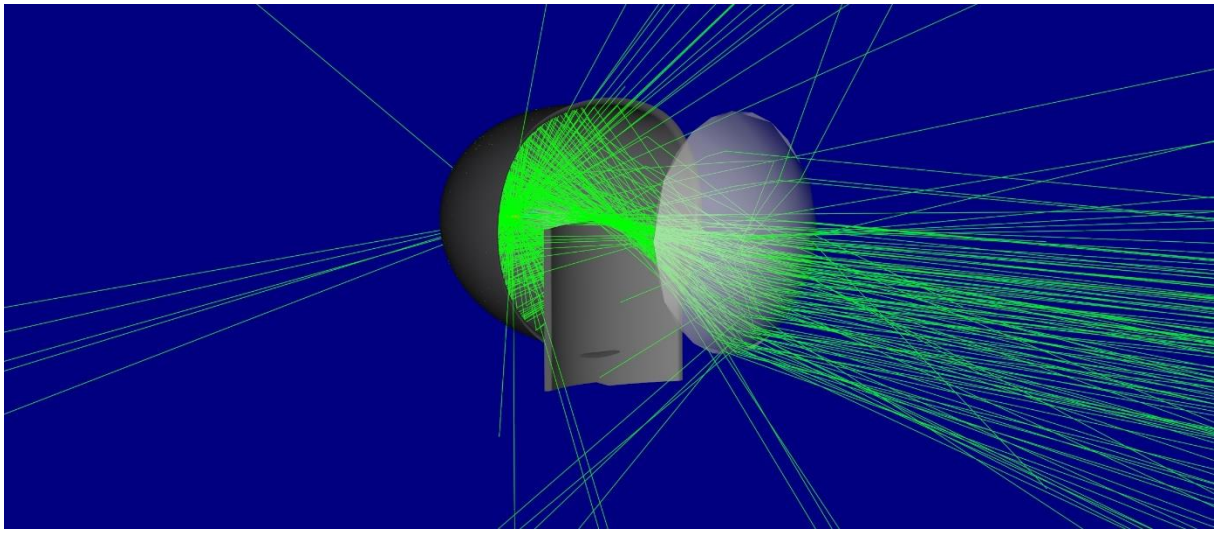

Figure 2: Example of RT using Helios. A light source souranded by a reflector element reflects the light rays onto the optical element to bundle the light onto the detector plane. An aperture shapes the light into a classical low beam distrinution.

©2024 by the authors. – Licensee Technische Universität Ilmenau, Deutschland.

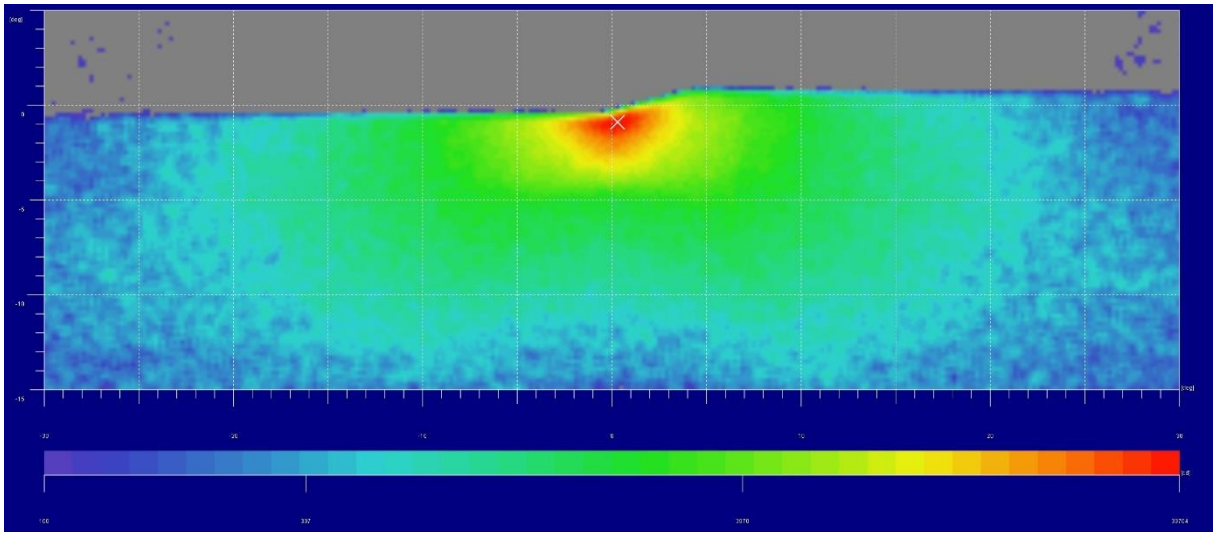

Figure 3: Illustration of the detected light intensity using Helios in an angel depding far field. The colorbar represents the intensity of the light field.

This principle is based on geometrical optics and uses a threedimensional Snellius law [10, 11]. Hence, the rays respectively the k-vector change the direction by hitting a material with a certain refractive indes. RT describes refractive optics that is generally valid for plane surfaces. If we consider surfaces with micro structures we can expect diffraction effects but those effects cannot be illustrated using a pure refracting tool [8, 12]. In addition, Helios is limited to the expression of material parameters. Therefore, a wave propagation method is introduced in the next section.

2.3 Introduction to the Finite-Difference Time-Domain Method

A well-known wave propagation method is FDTD. The FDTD method is based on Maxwell's curl equations and describes the propagation of electromagnetic waves in free space respectively in a medium with a certain refractive index and permittivity [4-8, 13, 14]. The relation of the time-depending electric and magnetic field vectors $\vec{E}(t)$ and $\vec{H}(t)$ [4, 15] is a result of Faraday's Law and Ampères Circuit Law regarding to [4-8, 13-16]. The necessary Maxwell equations with the connection between $\vec{E}(t)$ and $\vec{H}(t)$ are shown in Eq. (1) and Eq. (2).

$$\nabla \times \vec{E}(t) = -\frac{\partial \vec{H}(t)}{\partial t} \tag{1}$$

$$\nabla \times \vec{H}(t) = \frac{\partial \vec{E}(t)}{\partial t} \tag{2}$$

©2024 by the authors. – Licensee Technische Universität Ilmenau, Deutschland.

To add the corresponding material parameters for investigations of wave behavior not only in vacuum but also in a medium, we consider Maxwell's constitutive relations. These equations connect the electric $\vec{E}(t)$ and magnetic $\vec{H}(t)$ field with the electric $\vec{D}(t)$ and magnetic $\vec{B}(t)$ flux and the field constands ε_0, μ_0 as well as with the material specific parameters ε_r, μ_r. The form of the constitutive relations is shown in Eq. (3) and Eq. (4). [4-8, 13-16]

$$\vec{D}(t) = \varepsilon_0 \varepsilon_r \vec{E}(t) \tag{3}$$

$$\vec{B}(t) = \mu_0 \mu_r \vec{H}(t) \tag{4}$$

Since Eq. (1) and Eq. (2) are coupled partial differential equations (PDEs), a discrete solver for the numerical solution of Maxwell's curl equations is used. Considering a threedimensional problem, we have spatial derivatives along each space direction and a temporal derivation of the fields. In simulation approaches, the electric field and magnetic field $\vec{E}(t)$ and $\vec{H}(t)$ is shifted by a half unit cell in each direction and also shifted by a half time step in time. The spatial deviation of the constructed unit cells for $\vec{E}(t)$ and $\vec{H}(t)$ can be visualized using the Yee algorithm illustrated in Fig. 1 [14]. Here, the field components along the axes create a coupled cubic unit cell [14, 17].

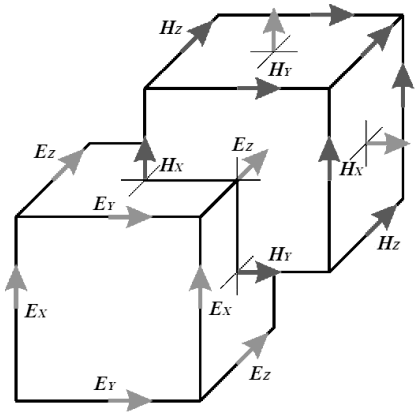

Figure 4: Position of the electric $\vec{E}(t)$ and magnetic $\vec{H}(t)$ field vector components about a cubic unit cell of the Yee space lattice. Each field defines a own unit cell shifted by a half grid step in every dimension to each other. [14, 17]

Based on the nature of PDEs, physical sensible boundary conditions must also be taken into account [18]. For periodic materials with an infinite expansion across the simulation space, periodic boundary conditions are used [4-7]. On the other hand, for materials with a finite surface structure, absorbing boundary conditions are a physical sensible tool to implement. The convolutional perfectly matched layer boundary conditions consists of an absorbing functions at the outer bounds of the simulation space [4-7]. Using this principle, the Yee algorithm is completed and able to perfom a FDTD simulation for periodic and aperiodic

©2024 by the authors. – Licensee Technische Universität Ilmenau, Deutschland.

structures. This results in several statements about the wave behavior. We are able to understand the propagation of a electromagnetic wave considering the material interaction. We are also able to see the diffraction pattern in the near field for the reflected and transmitted wave parts. At least this method gives us the field parts scattered in each reflection and transmission diffraction order [8]. The additional possibilities offered by the FDTD method will be explored in the next section.

3 Methods

The FDTD method offers a portfolio of possibilities and applications a purely geometrical optic tool does not offer. In the following, examples are shown for an additional use of the FDTD algorithm excluding the fact of wave propagation studies.

3.1 S-Parameter retrieval from inhomogeneous Metamerials

The scattering parameter S describes the complex valued field parts when a plane wave get reflected or transmitted at the metamaterial [19]. Using these scattering parameters, a base is build for a expanded material analysis regarding to matertial specific parameters [19]. According to [19] equality between an inhomogeneous structure and a continuous material is assumed. We consider a procedure for the assignment of effective material parameters of an inhomogeneous structure consisting of a comparison of the scattered waves. This implies the complex transmission and reflection coefficients, from a planar slab of inhomogeneous material to the scattering from a theoretical continuous material [19]. Both parameters are necessary to calculate the S-parameters. [19, 20.] A S-parameter measurement for a symmetric homogeneous in Fig. 5, an asymmetric inhomogeneous in Fig. 6, and a symmetric inhomogeneous scattering object with a thickness of d in Fig. 7.

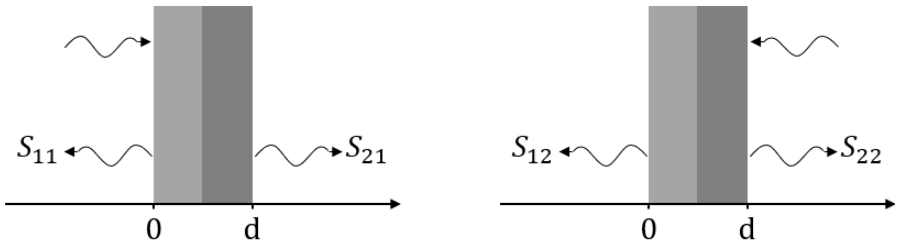

Figure 5: Illustration of the S-parameters for a symmetrix homogeneous scattering metamaterial on a 1D slab with thickness d. [19]

©2024 by the authors. – Licensee Technische Universität Ilmenau, Deutschland.

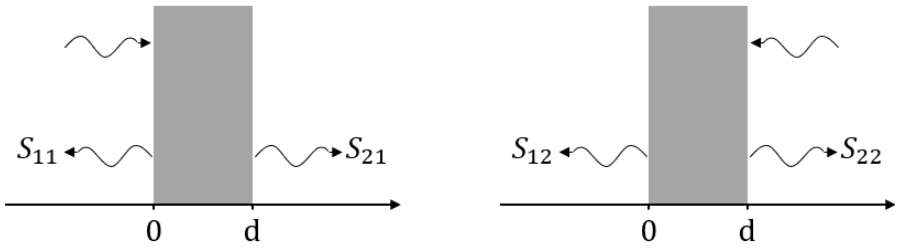

Figure 6: Showing of the scattering process an an asymmetrixc inhomogeneous metamatertral on a 1D slab with thickness d. [19]

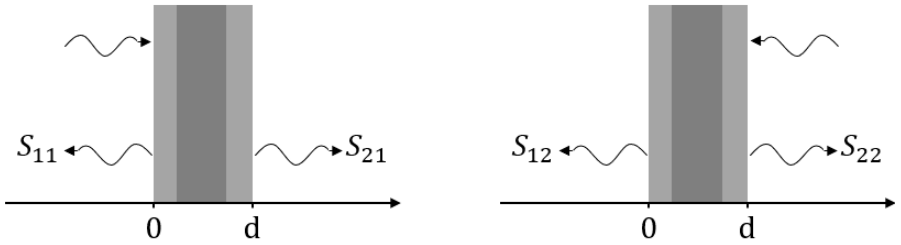

Figure 7: Illustration of the scattering on a symmetric inhomogeneous metamaterial on a 1D slab with thickness d. [19]

A S-parameter retrieval was initially used to characterize metamaterials with physically reasonable material properties described in [21] and in [22]. It is shown on the experiment of fabricated samples [19]. We consider materials shown in Fig. 6 and Fig. 7 since we observe inhomogeneous materials with different material parameters that affect the electromagnetic waves [19]. Here, the equivalent unit cell consists of at least two or more distinct materials that differ in their properties and field interactions. To understand this in more detail the S-parameters are defined on a mathematical basis. The general approach on the retrieval parameters for an inhomogeneous meta system is described. Smith et al. defines the S-parameter retrieval procedure as a prediction on the assumption that the analyzed structure can be replaced by a continuous material defined by the refractive index n and the impedance η [19]. We can expect that the retrieved parameters will not relate to the properties on the constituent components [19]. In relation to the propagation direction and the orientation of the unit cell the index n can be find defined by equation Eq. (5) or Eq. (6) depending on the propagation distance [19].

$$\cos(nkd) = \frac{1}{2S_{21}}(1 - S_{21}^2 + S_{11}^2) \tag{5}$$

$$\cos(nkd) = \frac{1}{2S_{21}}(1 - S_{22}^2 + S_{21}^2) \tag{6}$$

©2024 by the authors. – Licensee Technische Universität Ilmenau, Deutschland.

To simplify the problem, a unit cell repeated infinitely perpendicular to the incident wave vector is assumed[19, 23]. Realizing this in the algorithm a Fourier transform for each component of the $\vec{E}(t)$-Field in the reflection and transmission regime is performed and this field parts are normalized by the source term that is injected into the simulation space [3, 7]. For the calculation of the corresponding reflection and transmission scattering parameters S_{11} and S_{21}, we use a second Fourier transform normalized by the size of the x-y-plane of the simulation space described by $N_x N_y$. This can be expressed by the following in Eq. (7) and Eq. (8):

$$S_{11} = \mathrm{conj}\left(\sqrt{\left(\frac{\mathfrak{F}(E_{x,ref})}{N_x N_y}\right)^2 + \left(\frac{\mathfrak{F}(E_{y,ref})}{N_x N_y}\right)^2 + \left(\frac{\mathfrak{F}(E_{z,ref})}{N_x N_y}\right)^2}\right) \tag{7}$$

$$S_{21} = \mathrm{conj}\left(\sqrt{\left(\frac{\mathfrak{F}(E_{x,trn})}{N_x N_y}\right)^2 + \left(\frac{\mathfrak{F}(E_{y,trn})}{N_x N_y}\right)^2 + \left(\frac{\mathfrak{F}(E_{z,trn})}{N_x N_y}\right)^2}\right) \tag{8}$$

For further calculation of the Fresnel reflection coefficient r,first a so called inter-media parameter X_r is defined [3, 7]. Here, X_r is expressed in terms of the previously calculated scattering parameter S_{11} and S_{21} shown in Eq. (9) according to [3, 7, 19].

$$X_r = \frac{\left(1 - S_{21}^2 + S_{11}^2\right)}{2S_{11}} \tag{9}$$

The resulting Fresnel reflection can be calculated using this inter-media parameter in Eq. (10) [3, 7, 19].

$$r = X_r \pm \sqrt{X_r^2 - 1} \tag{10}$$

Using this Fresnel reflection parameter r we are able to calculate the corresponding transmission coefficient t which is described in Eq. (11) [3, 7, 19].

$$t = \frac{S_{11} + S_{22} - r}{1 - (S_{11} + S_{21})\, r} \tag{11}$$

To achieve the effective refractive index n_{eff} of the metamaterial and the corresponding impedance η we consider the wave vector in free space $k_0 = \frac{2\pi\omega}{c_0}$ and the free space impedance $\eta_0 = \sqrt{\frac{\epsilon_0}{\mu_0}}$ [3]. Using the r and t reflection and transmission parameter, those properties are expressed shown in Eq. (12) and Eq. (13) [3, 7, 19],

$$n_{\mathrm{eff}} = \frac{\ln(t)}{ik_0 a} \tag{12}$$

©2024 by the authors. – Licensee Technische Universität Ilmenau, Deutschland.

$$\eta_{\text{eff}} = \frac{\eta_0(1+r)}{1-r} \tag{13}$$

where a corresponds to the size of the unit cell. In a last step we use the calculated effective refractive index n_{eff} and impedance η to calculate the effective permittivity and permeability $\epsilon_{r,\text{eff}}$ and $\mu_{r,\text{eff}}$. This corresponds to the equations Eq. (14) and Eq. (15).

$$\epsilon_{r,\text{eff}} = \frac{n_{\text{eff}}\,\eta_0}{\eta} \tag{14}$$

$$\mu_{r,\text{eff}} = \frac{n_{\text{eff}}\,\eta}{\eta_0} \tag{15}$$

These parameter result in new possibilities to investigate the metamaterial not only regarding to the corresponding diffraction pattern and the field parts reflecting and transmitting in different diffraction orders. With this material analysing approach it is possible to understand the reflection and transmission behavior of the wave vor different frequencies. In case of a real material a high value of loss inside the metamaterial correspondes to a negative refractive index [19, 24, 25]. In the following the S-parameter retrieval of the reconstructed split ring resonator in [85] is compared to Smith et. Al.. For a qualitative investigation of material parameters we assume the split ring resonator from [19] with an edge length of 2.5 mm. The corresponding metametrial contains the same dimensions in x- and z-direction, only the material thickness differs by a height of 0.25 mm. The base for the metamaterial consists of a relative permittivity of $\epsilon_r = 4.4$ and an absorption coefficient of δ = 0.02. On the side facing away from us, we have a metal striped wire with a length of the entire unit cell and a width of 0.14 mm. The outer metal striped resonator rings has a length of 2.2 mm and a width of 0.2 mm. The inner ring consists of a length of 1.5 mm and has the same width of 0.2 mm. Both rings are build from the center of the unit cell in x- and z-direction. Each ring has a gap with a size of 0.3 mm. Both, the metal striped wire on the back side and the metal striped resonator at the front side, contain a conductivity of σ = 5.8 × 107 Ωm. Within this simulation and calculation of the scattering parameter and effective property values of the material, a plane wave propagating along the z-axis from top to bottom of the metamaterial is considered. Using FDTD simulations, we are able to investigate the magnitude scattering parameters S_{11} and S_{21} in Fig. 8, the corresponding phase response in Fig. 9, the effective refractive index $\text{n}_{\text{eff}}(\omega)$ and impedance $\eta_{\text{eff}}(\omega)$ in Fig. 10 and Fig. 11 and material parameter interacting with the incident wave, the permittivity ϵ_{eff} as well as μ_{eff} in Fig. 12 and Fig. 13. In comparison to the results of Smith et Al. in [19], the S-parameter retrieval results shown in Fig. 8-13 are very similar to the calculation using the commercial software HFSS (Ansoft), a finite-element-based electromagnetic mode solver used by Smith et. Al.. Each material parameter is shown for a frequency sweep in an interval from 1 GHz up to 20 GHz. First, the similarities to [19] are

©2024 by the authors. – Licensee Technische Universität Ilmenau, Deutschland.

considered. The material specific effects occur around a frequency of 10 GHz in comparison to the simulation using HFSS (Ansoft). The S-parameters and the associated phase profile exhibited only minor deviations from the commercial calculations. For the material-specific parameters that interact with the incident wave field, a similar trend across the frequency interval as reported in [19] is observed. However, discontinuities within the plot are also noted. If we shift the discontinuities to create a smooth plot, the resulting trend aligns closely with the previously reported results by Smith et. Al.. The cause of this discontinuities has to be disussed. Compared to the results in [19] the code is verified in rigorous ways, so numerical inaccurancies can be ruled out. Unlike commercially available simulation tools that typically import geometries via CAD models, our approach involves approximatively reconstructing the geometry.

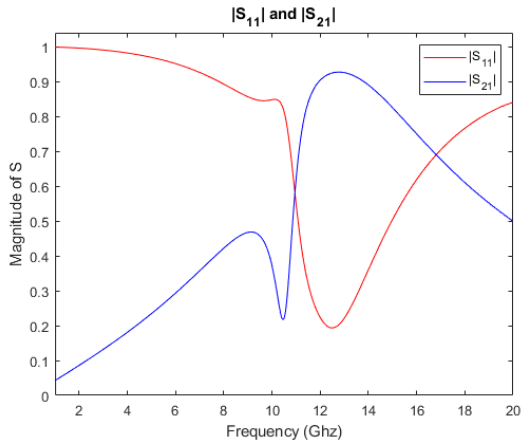

Figure 8: Magnitude of the scattering Parameter S_{11} and S_{21}.

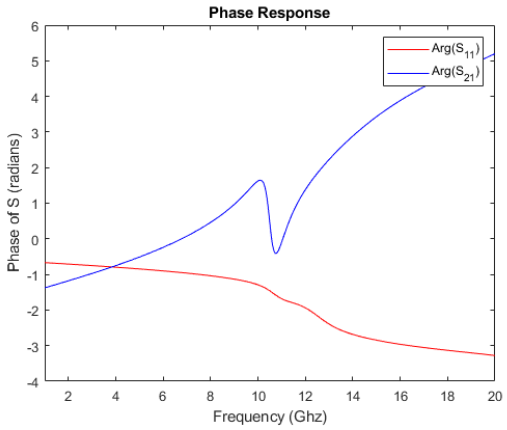

Figure 9: Corresponding angle of: Parameter S_{11} and S_{21}.

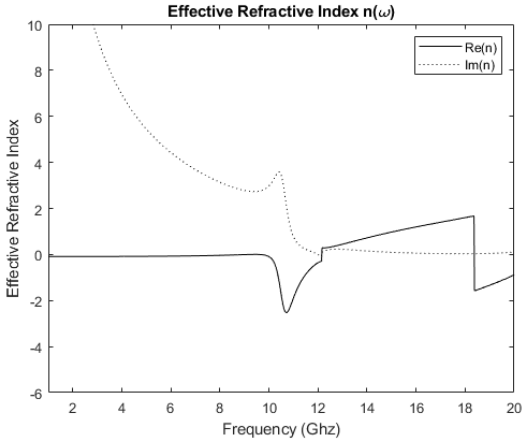

Figure 10: Real and imaginarypart of the effective refractive index.

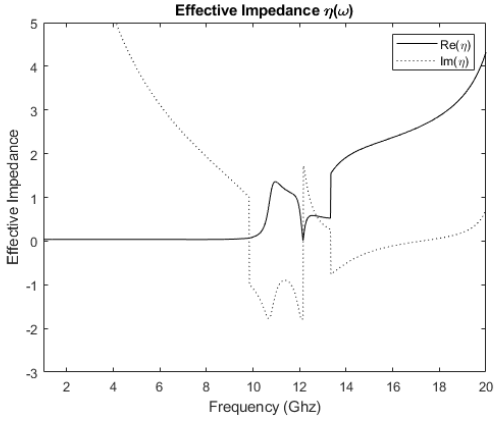

Figure 11: Real and imaginarypart of the effective impedance.

©2024 by the authors. – Licensee Technische Universität Ilmenau, Deutschland.

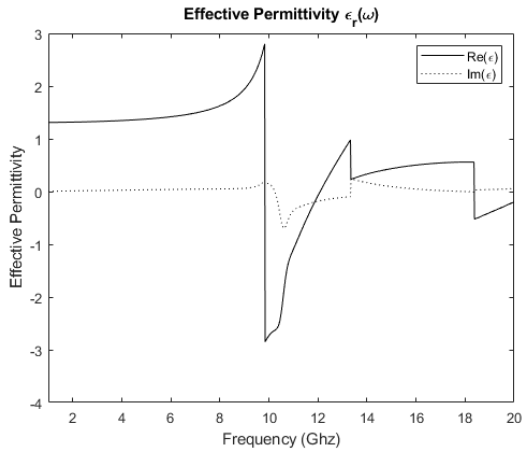

Figure 12: Real and imaginarypart of the effective permittivity.

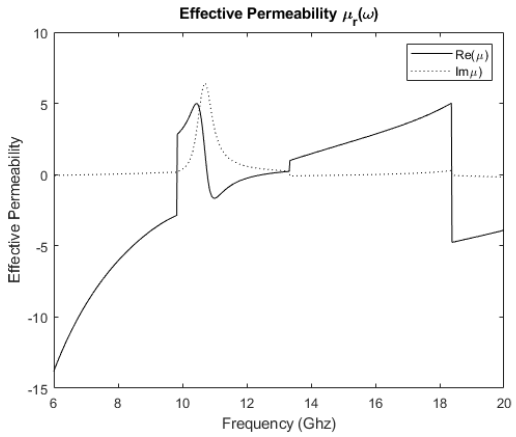

Figure 13: Real and imaginarypart of the effective permeability.

To discuss these geometric discrepancies in detail, the structure of the split ring resonator reconstructed in MATLAB is compared to the geometry described in [19]. Fig. 14 shows the geometry of a single unit cell of the resonator. In comparison to the reconstructed geometry recreated using MATLAB in Fig. 15, obvious differences in the inner corners of the resonator rings arw visible. These small but significant deviations to the original CAD model could lead to such difference.

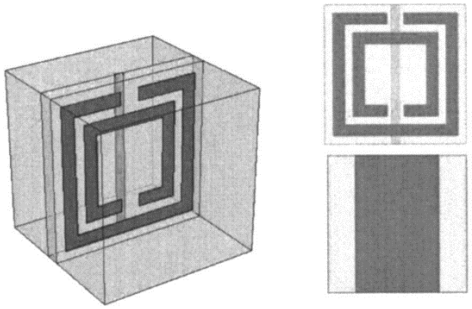

Figure 14: CAD Model by Smith et Al. [19]

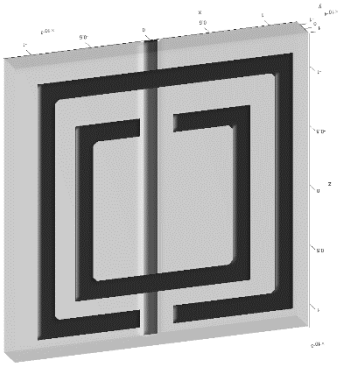

Figure 15: Reconstruction using MATLAB

Moreover, the conservation of energy is another indicator for the correctly functioning numerical simulation while the discrepancies are happening due geometry. Since this metamaterial simulation include intensity loss it is feasible to expect conversation of less then 100 %. Instead, we can expect that areas where we observe a peak in the imaginary part of the refractive index and a negative real part in Fig. 10, correspond to regions with a high loss rate. Fig. 16 shows the transmitted and reflected field part in solid blue and red and the accumulation of these part in a dotted black line.

©2024 by the authors. – Licensee Technische Universität Ilmenau, Deutschland.

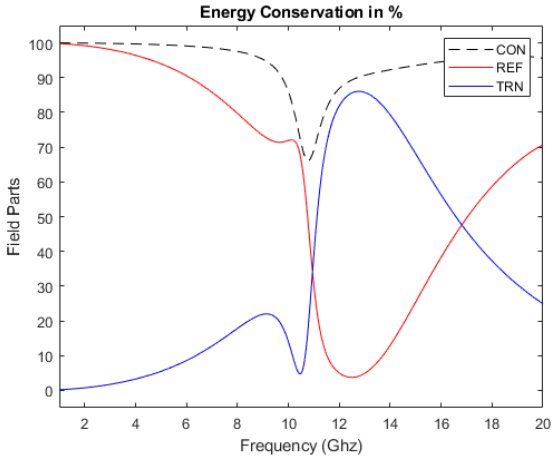

Figure 16: Visualization of the detected reflected and transmitted field normalized to 1 over the frequency spectra of 1 GHz up to 20 GHz. At around 10 GHz we observe an anomaly caused by the loss of the metamaterial for this specific frequency range.

©2024 by the authors. – Licensee Technische Universität Ilmenau, Deutschland.

3.2 Investigation of Scattering Field Part in higher Diffraction Orders

Another way to characterize geometries in the FDTD method is to divide the scattered wave into reflective and transmissive components relative to the input wave, regardless of the S-parameters. For this purpose, an analysis of a classical diffraction grating orientated along the x- and y-direction is examined. Furthermore, a structure with small antennas at the surface corresponding to a meta optical device and a hole structure is analysed. These diffractive elements are shown in Fig. 17-20.

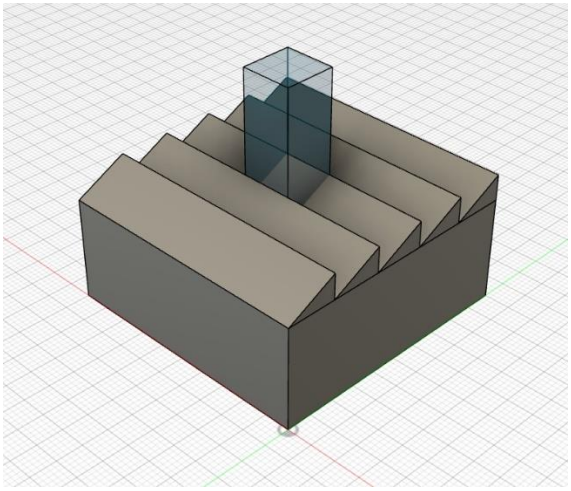

Figure 17: Diffraction grating orientated along X

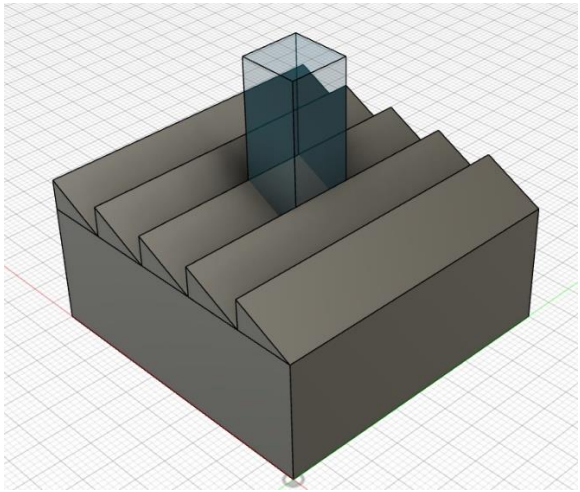

Figure 18: Diffraction grating orientated along Y

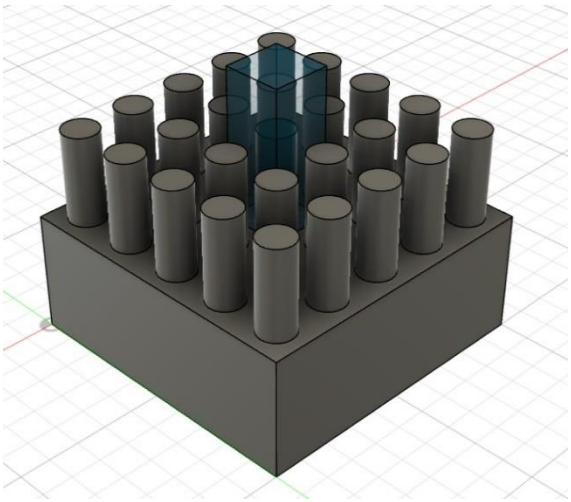

Figure 19: Meta optical surface

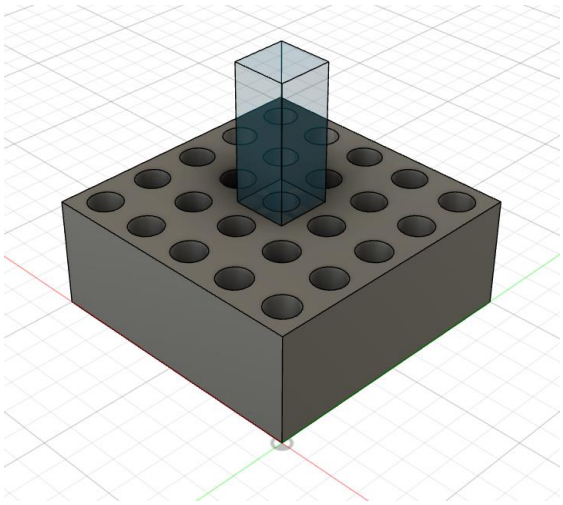

Figure 20: Surface with periodic holes

Since all these structure shown in Fig. 17-20 are periodic, a unit cell to simulate the wave behavior and scattering is considered. At the x- and y-bounds local periodic boundary conditions are used and at the top and bottom parallel to the incident wave along the z-axis we have PML boundary conditions [3]. Starting with the diffraction grating illustrated in Fig. 17, for such a structure a scattering along the x-axis can be considered since the y-axis is constant.

©2024 by the authors. – Licensee Technische Universität Ilmenau, Deutschland.

Vice versa there are the expectations for the diffraction grating shown in Fig. 18, since only the orientation is changed. The material parameters and size is equal for both cases. Here, a simulation space of 800 × 800 × 1500 nm is defined containing a grating with an angel of 26.57°. The Material consists of a refractive index of 1.52. Each simulation is done using an incident wave field of 600 nm. Table 1 and Table 2 show the corresponding scattering values for higher diffraction orders.

Tabelle 1: Reflection in each diffraction order along X. Total reflection 7.60%.

Order	m=-2	m=-1	m=0	m=1	m=2
n=-2	0	0	0	0	0
n=-1	0	0	0	0	0
n=0	0	0.013%	4.345%	3.246%	0
n=1	0	0	0	0	0
n=2	0	0	0	0	0

Tabelle 2: Transmission values in each diffraction order along X. Total transmission 99.15%.

Order	m=-2	m=-1	m=0	m=1	m=2
n=-2	0	0	0	0	0
n=-1	0	0	0	0	0
n=0	0.005%	15.619%	55.902%	15.104%	12.523%
n=1	0	0	0	0	0
n=2	0	0	0	0	0

Accumulated, a total field value of 106.76 % is detected. This is no sensible results since the diffraction grating is not aa field amplifier. However, in case of numerical inaccuracies and the total number of iteration to a certain threshold of remaining field parts within the simulation space, it is possible to receive greater than 100 % of energy. Table 3 and Table 4 show corresponding reflection and transmission parts for each diffraction order for the y-orientated grating shown in Fig. 18.

Tabelle 3: Reflection in each diffraction order along Y. Total reflection 6.32%.

Order	m=-2	m=-1	m=0	m=1	m=2
n=-2	0	0	0	0	0
n=-1	0	0	0.03%	0	0
n=0	0	0	5.24%	0	0
n=1	0	0	1.05%	0	0
n=2	0	0	0	0	0

Tabelle 4: Transmission values in each diffraction order along Y. Total transmission 93.84%.

Order	m=-2	m=-1	m=0	m=1	m=2
n=-2	0	0	0.49%	0	0
n=-1	0	0	8.96%	0	0
n=0	0	0	64.52%	0	0
n=1	0	0	15.90%	0	0
n=2	0	0	3.97%	0	0

©2024 by the authors. – Licensee Technische Universität Ilmenau, Deutschland.

In total a energy conversation of 100.16 % is received. This result is accurate to the expectations of 100 %. For the next example, a stricture with periodic antennas shown in Fig. 19 is assumed. We still consider a simulation space of 800 × 800 × 1500 nm for the the unit cell. The dimensions of the antenna correspond to a radius of 300 nm with a height of 500 nm and a material specific refractive index of 1.52. The reflected and transmitted field parts are listed in Table 5 and Table 6.

Tabelle 5: Reflection in each diffraction order for the antenna. Total reflection 4.72%.

Order	m=-2	m=-1	m=0	m=1	m=2
n=-2	0	0	0	0	0
n=-1	0	0	0.63%	0	0
n=0	0	0.41%	2.65%	0.41%	0
n=1	0	0	0.63%	0	0
n=2	0	0	0	0	0

Tabelle 6: Transmission values in each diffraction for the antenna. Total transmission 95.42%.

Order	m=-2	m=-1	m=0	m=1	m=2
n=-2	0	0.0005%	0.12%	0.0005%	0
n=-1	0.0014%	4.44%	13.09%	4.44%	0.0014%
n=0	0.76%	12.72%	24.10%	12.75%	0.77%
n=1	0.0014%	4.53%	13.13%	4.46%	0.0014%
n=2	0	0.0005%	0.12%	0.0005%	0

For this specific case an energy conversation of 100.14 % is received. For the last example a similar case to the antenna structure is considered. We still observe a simulation space of 800 × 800 × 1500 nm for a unit cell and instead of antennas the scattering behavior at a hole structure with a radius of 300 nm, a depth of 500 nm and a material specific refractive index of 1.52 is analysed. The reflected and transmitted field parts are listed in Table 7 and Table 8.

Tabelle 7: Reflection in each diffraction order for the hole structure. Total reflection 2.29%.

Order	m=-2	m=-1	m=0	m=1	m=2
n=-2	0	0	0	0	0
n=-1	0	0	0.28%	0	0
n=0	0	0.30%	1.28%	0.30%	0
n=1	0	0	0.27%	0	0
n=2	0	0	0	0	0

©2024 by the authors. – Licensee Technische Universität Ilmenau, Deutschland.

Tabelle 8: Transmission values in each diffraction order for the hole structure. Total transmission 95.05%.

Order	m=-2	m=-1	m=0	m=1	m=2
n=-2	0	0.001%	0.41%	0.001%	0
n=-1	0.002%	5.26%	4.50%	5.14%	0.002%
n=0	0.85%	13.87%	35.73%	13.80%	0.82%
n=1	0.002%	5.20%	4.5%	5.33%	0.002%
n=2	0	0.001%	0.40%	0.001%	0

For this example a total energy of 98.49 % is obtained. The scattering of each of these structures converges to the expectations. These results can be compared to a Rigorous Coupled Wave Approximation (RCWA) and this shows the scope of possibilities using a FDTD simulation for different geometries and materials [3, 7].

3.3 Band Structure Analysis of a Photonic Crystal

For the last example of possibilities using FDTD simulations, a lattice of a photonic crystal consisting of silicon with a relative permittivity of 12.25 is considered [26]. At first, a cubic unit cell with a width of $a = 1$ µm is defined. Since the photonic crystal is defined by the hole of air inside the unit cell, we charatirize this spherical space with a radius of 0.6 µm. The material cell is shown in Fig. 21.

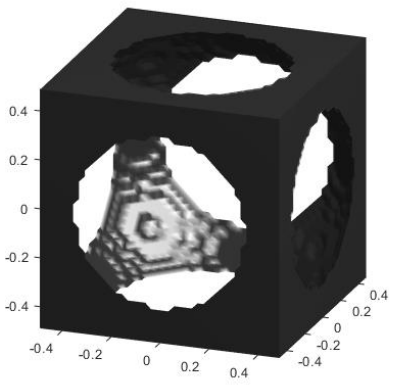

Figure 21: Illustration of the Wigner-Seitz unit cell containing the silicon photonic crystal with a total length of 1 µm in each dimension. The spherical spaces contains a radius filled with air by 0.6 µm.

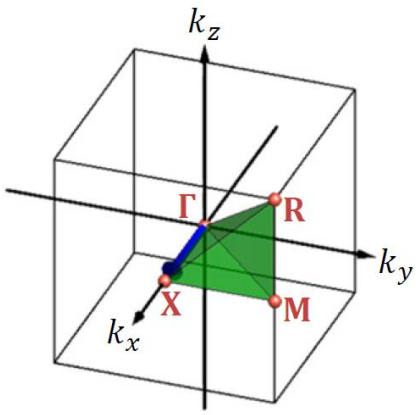

Figure 22: Representation of the unit cell in reciprocal space defining the axis by $\vec{k}_x$, $\vec{k}_y$ and $\vec{k}_z$. Here the energy points M →Γ→R→X within the Brillouin zone are shown. [7]

For building the Brillouin zone, the lattice vectors along the axis so, $\vec{t}_1$, $\vec{t}_2$ and $\vec{t}_3$ correspondes to the unit vectors along x, y and z need to be defined. Since the Brillouin zone is a reciprocal cell equivalent to the Wigner-Seitz primitive unit cell in real space, we have to calculate the reciprocal lattice vectors $\vec{T}_{1,2,3} = \frac{2\pi}{a}\vec{t}_{1,2,3}$ [27]. This results in a cubic unit cell again. Now, the

©2024 by the authors. – Licensee Technische Universität Ilmenau, Deutschland.

smallest volume of space in the Brillouin zone that completely characterizes the lattice is considred. This space is called irreducible Brillouin zone (IBZ) [7]. The key symmetry points are the vertecies of the IBZ. Band extreemes usually occur at the symmetry points. We consider the center of the unit cell Γ, this point is defined by $\Gamma = 0$. The center on the front surface is in a distance of half a unit cell along the k_x-direction. This point is defined by $X = 0.5\,\vec{T}_1$. The corner point on the k_x-k_y-plane is definded by $M = 0.5\,\vec{T}_1 + 0.5\,\vec{T}_2$. The last point of the unit cell defies the corner point of the unit cell $R = 0.5\,\vec{T}_1 + 0.5\,\vec{T}_2 + 0.5\,\vec{T}_3$ [7, 27]. There is no convention for choosing a path around the IBZ. For this simulation using FDTD a path over M →Γ→R→X is chosen. This path is shown in Fig 22. Using an analysis of the power spectral density over a range from zero up to 0.18 GHz the spectral peaks on a logarithmic scale are ionvestigated. Following the path M →Γ→R→X along the Bloch vector $\vec{\beta}$ the normalized frequency $\omega = \frac{a}{\lambda_0}$ is calculated and the resulting band diagram is shown in Fig 23.

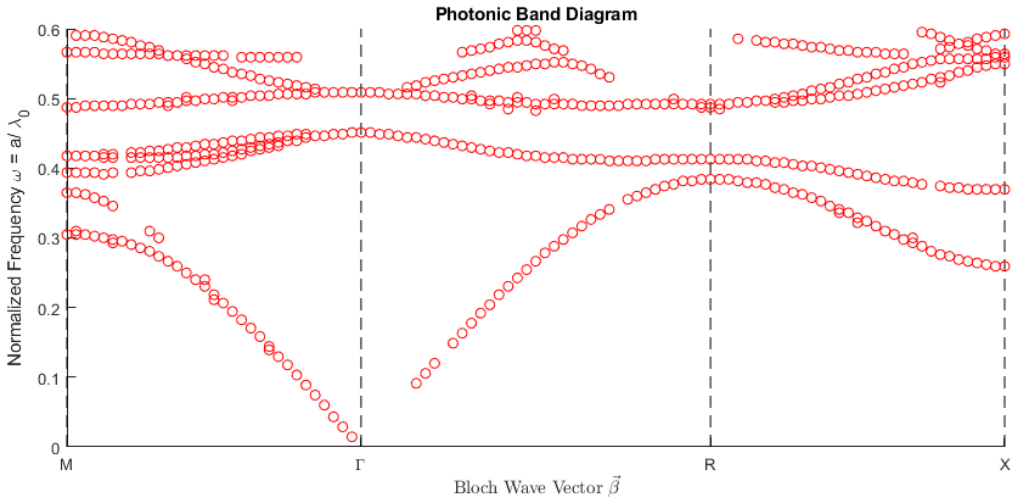

Figure 23: Photonic band diagram for a silicon photonic crystal. On the x-axis we present the path through the Brillouin zone by M →Γ→R→X.. The y-axis represents the normalized frequency ω equaivalent to the band energy. The gap between the conduction and valenz band shows the gap energy we need to add to the system for a passing from the valenz into the conduction band.

It is possible to use FDTD for a band analysis of semiconductor materials. However, this method contains numerical unaccurancies in the fact that some points in the band diagram, as shown in Fig 23, are vanished or not regocnized as a peak within the power spectral density analysis. For a rough understanding, this method could be used but we should take the computation time into account as well. Since FDTD based on the solution of Maxwell's equations there is a great scope of iterations for each point within Fig. 23. Numerical methods e. g. a Plane Wave Expansion Method is probably a more sensible method to use for this special use case with respect to the expense and computation time. [7]

©2024 by the authors. – Licensee Technische Universität Ilmenau, Deutschland.

4 Conclusion and Outlook

Concluding the result, FDTD offers several methods to expand the RT tool by Helios. Using this method the material defining parameters e. g. the effective permittivity and permebility, the effective refractive index and impedance can be analysed. All these parameters were calculated using the scattering parameters resulting from an S-parameter retrieval. With the results of the S-parameter retrieval the inhomogeneous metametrial is characterized. With a further attempt, a unit cell using periodic boundary conditions to calculate a diffraction grating and a meta optic structure with periodic antennas and a periodic hole structure is created. Using FDTD simulations the scattering parts in different diffraction orders according to energy conservation are investigated. Those results can be confirmed using RCWA simualtions. In the last example the photonic band structure of a photonic crystal with a relative permittivity of 12.25 according to silicon is calculated. Over a path of M →Γ→R→X through the IBZ we calculated the band energy and were able to see the band gap between the valence and conduction band. The FDTD method also gives us a possibility to investigate the energies within a semiconductor material e. g. silicon. In general we have a bundle of possibilities using only one single method initialiy developed to understand wave propagation through a material. Combining RT with FDTD we have a very powerful tool for optical analysis of material and light propagation.

©2024 by the authors. – Licensee Technische Universität Ilmenau, Deutschland.

5 Bibliography

[1] Burkard Wördenweber, Jörg Wallascheck, Peter Boyce, Donald D. Hoffman “Automotive Lighting and Human Vision”, Springer Berlin, ISBN: 978-3-540-36697-3 (2007) DOI: https://doi.org/10.1007/978-3-540-36697-3

[2] Claude Leiner et al. “A Simulation Procedure Interfacing Ray-Tracing and Finite-Difference Time-Domain Methods for a Combined Simulation of Diffractive and Refractive Optical Elements”. In: Journal of Lightwave Technology32.6 (2014), pp. 1054–1062. doi: 10.1109/JLT.2013.2297411.

[3] Atef Z Elsherbeni and V Demir. The Finite-Difference Time-Domain Method for Electromagnetics with MATLAB® Simulations. Springer Verlag Berlin, Heidelberg, (2012). isbn: 978-1-89112-171-5.

[4] Raymond C. Rumpf. Electromagnetic and Photonic Simulation for the Beginners - Finite-Difference Frequency Domain in MATLAB®. Artech House Boston London, (2022). isbn: 978-1-63081-926-2.

[5] Raymond C. Rumpf. “Chapter Three - Engineering the Dispersion and Anisotropy of Periodic Electromagnetic Structures”. In: ed. by Robert E. Camley and Robert L. Stamps. Vol. 66. Solid State Physics. Academic Press, (2015), pp. 213– 300. doi: https://doi.org/10.1016/bs.ssp.2015.02.002.

[6] Raymond C. Rumpf. “Simple Implementation of Arbitrarily Shaped Total-Field/Scattered-Field Regions in Finite-Difference Frequency-Domain”. In:Progress In Electromagnetics Research B 36 (2012), pp. 221–248. doi: doi:10.2528/PIERB11092006.

[7] Raymond C. Rumpf. “Electromagnetic Analysis Using Finite-Difference Time Domain”. In: EM Possible EMP-5304 (2023). url: https://empossible.net/academics/emp5304/.

[8] A. Taflove and S.C. Hagness. Computational Electrodynamics: The Finitedifference Time-domain Method. Artech House antennas and propagation library. Artech House, (2005). isbn: 9781580538329. url: https://books.google.de/books?id=n2ViQgAACAAJ.

[9] Stephen D. Gedney. “Introduction to the Finite-Difference Time-Domain (FDTD) Method for Electromagnetics”. In: Springer Cham, (2011). isbn: 978- 1-608-45523-2. doi: https://doi.org/10.1007/978-3-031-01712-4.

[10] Glassner, Andrew S., An introduction to ray tracing. Morgan Kaufmann, (1989).

[11] Eugene Hecht. Optik. Berlin, Boston: De Gruyter, (2018). isbn: 9783110526653. doi:10.1515/9783110526653. url: https://doi.org/10.1515/ 9783110526653.

[12] Erwin G. Loewen and Evgeny Popov. Diffraction Gratings and Applications.Crc Press Inc, (1997). isbn: 978-0-8247-9923-6

[13] Fan Yang et al. “A simple and efficient FDTD/PBC algorithm for scattering analysis of periodic structures”. In: Radio Science 42.04 (2007), pp. 1–9.

[14] Kane S. Yee. “Numerical solution of initial boundary value problems involving maxwell’s equations in isotropic media”. In: IEEE Transactions on Antennas and Propagation 14.3 (1966), pp. 302–307. doi: 10.1109/TAP.1966.1138693.

©2024 by the authors. – Licensee Technische Universität Ilmenau, Deutschland.

[15] Wolfgang Nolting. Grundkurs Theoretische Physik 3 Elektrodynamik. Springer- Lehrbuch. Springer Spektrum Berlin, Heidelberg, 2013. isbn: 9783642379048. doi: https://doi.org/10.1007/978-3-642-37905-5.

[16] David J Griffiths. Introduction to electrodynamics. Pearson, 2013.

[17] Dzmitry M. Shyroki. “Modeling of Sloped Interfaces on a Yee Grid”. In: IEEE Transactions on Antennas and Propagation 59 (2011), pp. 3290–3295. url: https://api.semanticscholar.org/CorpusID:38140748.

[18] Wolfgang Arendt and Karsten Urban. “Neumann- und Robin-Randbedingungen”. In: Partielle Differenzialgleichungen: Eine Einf¨uhrung in analytische und numerische Methoden. Heidelberg: Spektrum Akademischer Verlag, 2010, pp. 219–244. isbn: 978-3-8274-2237-8. doi: 10.1007/978-3-8274-2237-8_7. url: https://doi.org/10.1007/978-3-8274-2237-8_7.

[19] D. R. Smith et al. “Electromagnetic parameter retrieval from inhomogeneous metamaterials”. In: Phys. Rev. E 71 (3 Mar. 2005), p. 036617. doi: 10.1103/PhysRevE.71.036617. url: https://link.aps.org/doi/10.1103/PhysRevE.71.036617.

[20] Joseph Ivin Thomas. “The classical double slit experiment–a study of the distribution of interference fringes formed on distant screens of varied shapes”.In: European Journal of Physics 41.5 (Aug. 2020), p. 055305. doi: 10.1088/1361- 6404/ab9afd. url: https://dx.doi.org/10.1088/1361- 6404/ab9afd.

[21] D. R. Smith et al. “Determination of effective permittivity and permeability of metamaterials from reflection and transmission coefficients”. In: Phys. Rev. B 65 (19 Apr. 2002), p. 195104. doi: 10.1103/PhysRevB.65.195104. url:https://link.aps.org/doi/10.1103/PhysRevB.65.195104.

[22] Tom Driscoll et al. “Free-space microwave focusing by a negative-index gradient lens”. In: Applied Physics Letters 88.8 (2006).

[23] David M Pozar. Microwave engineering: theory and techniques. John Wiley & Sons, (2021)

[24] David R Smith et al. “Composite medium with simultaneously negative permeability and permittivity”. In: Physical review letters 84.18 (2000), p. 4184.

[25] AA Zhilin and MP Shepilov. “Metamaterials with negative refractive index”. In: Journal of Optical Technology 75.4 (2008)

[26] A. B. Sproul, Green, M. A., and Zhao, J., “Improved value for the silicon intrinsic carrier concentration at 300 K”, Applied Physics Letters, vol. 57, p. 255, (1990)

[27] Gerd Czycholl. “Theoretische Festk¨orperphysik Band 2”. In: Berlin, Heidelberg: Springer Berlin Heidelberg, 2017. isbn: 978-3-662-53701-5. doi: https://doi.org/10.1007/978-3-662-53701-5.

©2024 by the authors. – Licensee Technische Universität Ilmenau, Deutschland.